Chapter 4

Role of defects AZO thin film deposited by spin coating

4.1 Introduction

Spin coating due to its simple operating procedure and easy thickness control during coating is being projected as a good alternative [222,223]. The concentration of precursor, pre and post-annealing procedure, the substrate, and the spinning speed are some of the important aspects which affect the electrical and optical properties of the deposited AZO thin films [28,224]. However, generally, spin-coated AZO films result in higher resistivity values when compared with techniques like spray pyrolysis or chemical vapor deposition. There are a few reports which do claim to achieve lower resistivity values; however, without substantiating the reasons. Tonny et al., [117] achieved resistivity of the order ~10^{-4} Ω-cm, which has been best reported so far by using high boiling point solvent 2-methoxyethanol, zinc acetate dihydrate (ZnAc) precursors, monoethanolamine as a stabilizer and Al nitrate nonahydrate as a dopant. However, this low resistivity was achieved with a micron-thick film, and the reported transmittance (~50%) was far less than the benchmark of 85%. Tang and Cameron [218] also reported resistivity in the order of ~10^{-4} Ω-cm, which is the lowest value achieved so far by a solution-based route, while using zinc acetate and aluminum nitrate or chloride as a dopant; however, no microstructural features and grain morphology was presented. Ohyama et al. [28] achieved resistivity in the order of ~10^{-3} Ω-cm for AZO thin films by using 2-

methoxy ethanol as a solvent; however, they did not report any optical properties such as transmittance, absorbance, or bandgap. Bandyopadhyay [225], on the other hand, described the optical properties of AZO films and their effect on bandgap; however, they did not mention the electrical properties of the AZO films. Nishio et al. [226] prepared c-axis oriented AZO films and also mentioned obtained resistivity ~10^{-3} Ω-cm; however, no further details about the measurements were mentioned. Several authors have reported a wide range of resistivity and transmittance values for AZO thin films via solution spin coating routes utilizing alcoholic as well as high boiling point solvents (such as 2-methoxy ethanol)[92]. To the best of our knowledge, there is no report correlating the dopant concentrations, structural features (such as microstructure, grain size, surface roughness), and defect states with optical and electrical properties for spin-coated films.

In this chapter, the microstructure, bandgap, defect states, and their correlation with the electrical and optical properties with varying Al concentration (0-3 at.%) are investigated. The resistivity in the order of 10^{-2} Ω-cm along with greater than 85% transparency was achieved in the films having 2 at.% Al doping.

4.2 Result and Discussion

4.2.1 X-ray diffraction

Pure ZnO and Al-doped ZnO precursor solutions were spin-coated on the glass substrate and annealed at 550°C. Crystallographic phase formation was confirmed by grazing incidence x-ray diffraction (GIXRD) at an incidence angle of 0.4°

(shown in **Figure 4.1**). XRD peak position matched with the standard pattern of the wurtzite phase of ZnO (JCPDS ref no: 79-027), which was also confirmed by earlier literature reports[28,218]. Generally, randomly distributed wurtzite phase of zinc oxide and doped zinc oxide thin films show (101) planes as the most intense XRD peak followed by the peaks corresponding to (100) and (002) planes. In the XRD patterns of Al-doped zinc oxide films (depicted in **Figure 4.1**), the peak positions were little shifted, while the most intense peak was at $2\theta=36.3°$ corresponding to the (101) planes. The intensity of the peaks in each XRD pattern was normalized against the (101) peak. The normalized integrated intensity of the (100), (002), and (102) peaks are listed in **Table 4.1**. The relative intensity of the (002) peak was observed to be 0.74 (normalized against the most intense (101) peak), which increased progressively to 0.89 when Al concentration increased to 3 at.%. This was much greater than 0.415, generally observed relative intensity of (002) for the randomly oriented crystalline films. This increase in relative peak intensity of (002) planes indicated that the films had a greater tendency to align along [002] on increasing Al concentration. It has earlier been concluded that a columnar growth along the c-axis orientation results in enhanced conductivity[218,226]. These results are consistent with earlier reports suggesting that the higher annealing and higher doping concentration favor c-axis orientation in the AZO films[28,218]**.** The ionic radius of Al^{+3} (0.51Å) is much smaller than Zn^{+2} (0.74Å). The substitution of Al^{+3} at Zn^{+2} positions in the lattice creates lattice strains, which eventually result in smaller crystallographic domains[74]. A substantial reduction in peak intensity and greater peak broadening was observed with an increase in Al concentration from 0 to 3 at.%. Broadening due to the crystallite size and the strain was calculated using

the Williamson-Hall method [227,228]. The strain increased progressively while the crystallite size decreased with increasing Al concentration (shown in **Figure 4.2**). For instance, the average crystallite size was about ~23.9 nm in pure ZnO films which reduced progressively to about ~17.9 nm for 3 at. % Al-doped ZnO films. On the other hand, the strain increased by an order from 0.0013 for the undoped sample to 0.0073 for 3 at. % Al-doped films. The reduction in crystallite size and grain size could be because of the introduction of aluminum at zinc sites, which introduced lattice strain. The lattice strain would accumulate on increasing the crystallographic domain size; as a result, on increasing doping levels, smaller crystallites were favored. No extra peak corresponding to pure alumina or zinc aluminates was observed in the XRD patterns. This indicates that any secondary impurity phase, if present, was well below the detection limit of XRD.

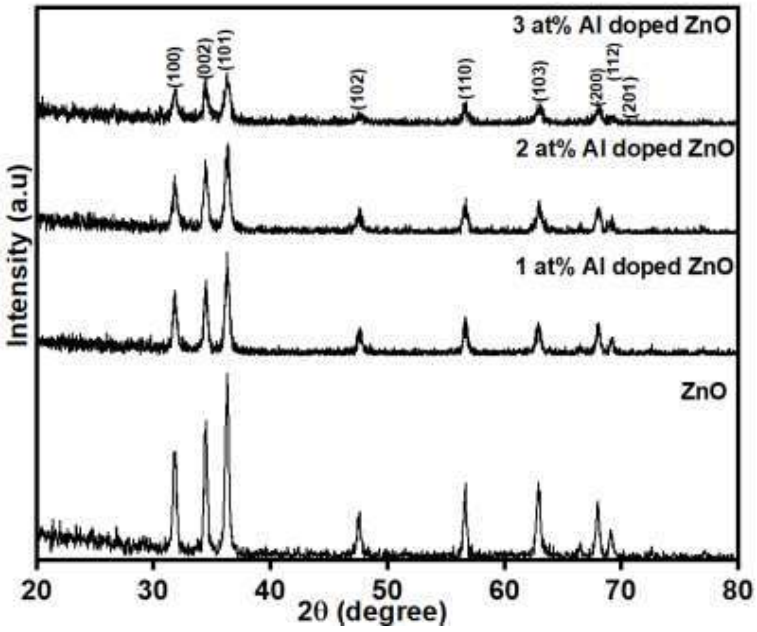

Figure 4.1 XRD pattern of pure ZnO and 1-3 at% Al-doped ZnO

Table 4.1 XRD peak intensity of zinc oxide and Al-doped ZnO films normalized relative to (101) and compared to zinc oxide random powder XRD peak intensity ratio

	Intensity ratio relative to (101)				
Crystallographic planes	ZnO* (Random)	ZnO 0 at% Al	ZnO 1 at% Al	ZnO 2 at% Al	ZnO 3 at% Al
(100)	0.56	0.58	0.63	0.64	0.69
(002)	0.41	0.74	0.73	0.81	0.89
(101)	1	1	1	1	1
(102)	0.21	0.26	0.27	0.29	0.24

*JCPDS Ref.Pattern-79-2205

4.2.2 Scanning electron microscopy

The morphology of the deposited films was analysed by HR-SEM. Secondary electron images of the films are depicted in **Figure 4.3** It was observed that films were largely uniform and continuous. It was also noticed that the grain size of the films decreased progressively with increasing Al concentration[64]. This trend was similar to the trend observed in crystallite size (shown in **Table 4.2**). Gaps between the grains were observed in pure ZnO films,

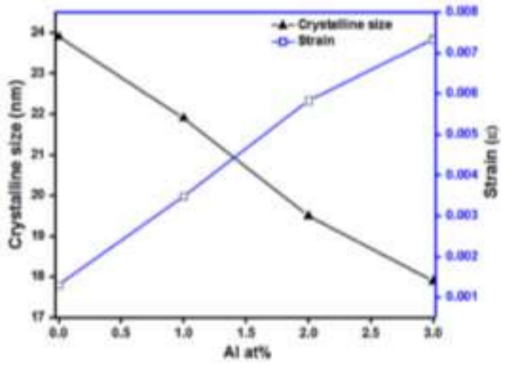

Figure 4.2 Crystalline size and strain as a function of Al doping concentration from 0 to 3 at.%

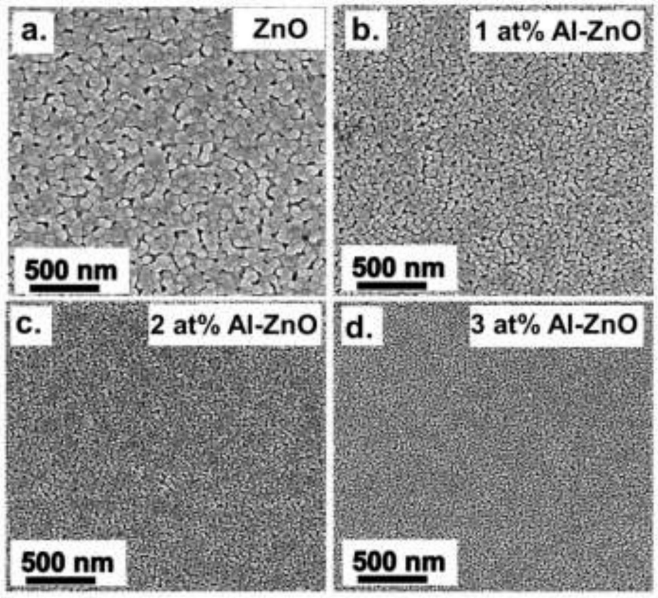

Figure 4.3 SEM images of ZnO doped with a) Pure ZnO b) 1 at.% Al c) 2 at.% Al d) 3 at.% Al

which reduced markedly with increasing aluminum concentration (0-3 at.%), resulting in increased density of the films (**Figure 4.3**).

Table 4.2 Crystalline size and grain size of wurtzite structure planes of (0-3) at.% Al-doped ZnO

	Crystalline size (in nm)	
Aluminum Doping (atomic %)	The average Crystallite size (nm)	Grain size from SEM (nm)
0	23.9	85
1	21.9	39
2	19.5	35
3	17.9	25

Film thickness and morphology are important parameters, which can affect the transparency and electrical properties of the TCOs. On increasing film thickness, generally, both resistivity and transparency decrease [117,229]. The thickness of the films measured using M-probe was about ~150 nm.

4.2.3 Scanning kelvin probe microscopy

Charge concentration and work function of films play an important role in determining the overall conductivity of the films. Generally, uniform work function

over the film surface is said to be ideal for achieving good conductivity at macro scales. Due to its inherent nanometric spatial resolution, SKPM has been

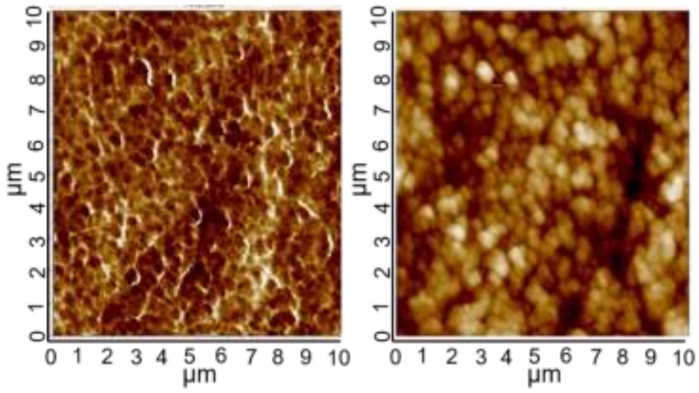

Figure 4.4 Two-dimensional a) contact potential difference V_{CPD} image of 2 at. % Al-doped ZnO b) 2D image of surface roughness of 2 at. % Al-doped ZnO

successively used to probe non-uniform doping distribution at the nanoscale[230]. The relative work function can be estimated by measuring contact potential against a reference like Si, Ge, etc. The areas having greater contact potential differences such as grain boundaries would work as a trap and tend to hinder the movement of charge carriers resulting in increased resistivity. To examine the contact potential distribution over the microscopic level, scanning kelvin probe microscopy of the AZO films having 2 at. % Al doping was carried out. Since the electron affinity of the sample and the work function of Ag remain constant for a fixed temperature, the contact potential difference (V_{cpd}) can be assumed to be proportional to the charge concentration. The contact potential difference was measured over an area of 10x10 µm is depicted in **Figure 4.4**. The grain boundaries appear brighter than the grain interior, indicating that the contact potential difference was greater at grain

boundaries when compared to the interior of the grains. This indicates that work function and in turn, the charge concentration were much greater at the grain boundaries. The higher contact potential difference regions would act as traps and could result in reduced conductivity. This difference was attributed to the greater defect concentration at the grain boundaries such as oxygen, the formation of alumina, and zinc vacancies acting as electrically active deep levels[230,231].

4.2.4 Optical properties

To characterize the optical properties of the deposited Al-doped ZnO films, UV-vis spectroscopy was carried out in the wavelength range 350-800 nm (depicted in **Figure 4.5**). For the TCO to be applicable in solar cells, transparency in the visible and near IR spectral range is of prime importance. The transparency of the films was determined by recording transmittance spectra in the wavelength range of 350-800 nm. Transparency of all the films was greater than ~85% in the visible-IR wavelength range of 350 nm to 800 nm **Figure 4.5a**. The absorption edge of the films exhibited a blue shift with increasing doping levels from undoped to1 to 3 at.% Al. Tauc plot of Al-doped zinc oxide thin films is depicted in the inset of **Figure 4.5b**. The bandgap as a function of dopant concentration is listed in **Table 4.3**. The bandgap of pure ZnO film was determined to be 3.14 eV, which increased progressively with Al doping to 3.19 eV for 3 at. % doped films. This increase in the bandgap is consistent with earlier reports[231,232]. The increase in the optical bandgap with increasing Al concentration was attributed to the increasing concentration of electrons near the conduction band, which shifts the Fermi level closer to the conduction band[39,233].

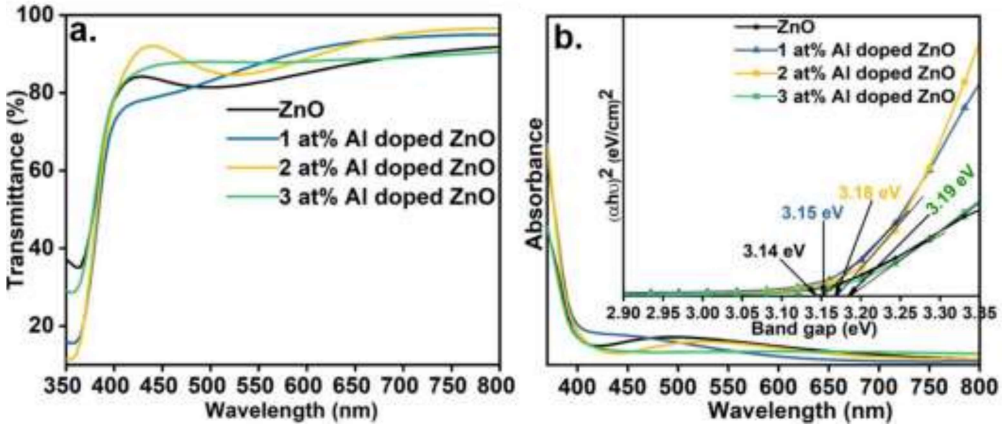

Figure 4.5 Transmittance a) absorbance and Tauc plot (inset) b) of Al-doped ZnO films having ZnO and 1 to 3 at. % Al concentration

Table 4.3 Bandgap of ZnO and 1 to 3 at.% Al-doped zinc oxide films

Dopant (at % Al)	Bandgap(eV)
0	3.14
1	3.15
2	3.18
3	3.19

4.2.5 X-ray photoelectron spectroscopy

XPS was performed for 1 at. % Al-doped ZnO thin film to get insight into the Zn and Al oxidation state. A detailed scan of the peaks corresponding to the Zn 2p and Al 2p was done to analyze the oxidation state of Zn and the dopant Al. The doublet peaks corresponding to Zn $2p_{3/2}$ and $2p_{1/2}$ were observed at 1021.6±0.1 eV and 1044.7±0.1 eV, respectively (shown in **Figure 4.6a**). Having an energy difference

of 23.10 eV which states that ZnO formation has taken place[234]. The Zn $2p_{3/2}$ peak was shifted by about $\Delta E_{Zn} = 0.1$ eV from that of elemental Zn (which should be at 1021.5 eV), indicating that the zinc was in the oxidized state. This was in good agreement with the earlier reported binding energies for the Zn2p peaks of AZO[33,106,235]. On closer inspection of Zn $2p_{3/2}$ peaks, a shoulder-like hump could be observed towards the higher energy side of the peaks. The energetic location of these shoulders (at 1023.0±0.17 eV) (as shown in **Figure 4.6b**) suggested that some amount of Zn was at a slightly higher oxidation state than ZnO. This is an important observation, which was attributed to the Zn atoms occupying interstitial sites and surrounded by more than one oxygen atom at the same time. This was direct evidence of the presence of zinc atoms at the interstitial sites. The presence of Zn at the interstitial site was also confirmed by the photoluminescence (PL) of the AZO films (**Figure 4.8b**). The appearance of Al 2p peaks cantered at 74.0 ± 0.1 eV in AZO films indicates that Al doping successfully took place into the ZnO lattice through the substitution of Al^{+3} at the Zn^{2+} sites [106,236] (shown in **Figure 4.7**). The Al2p peak could be deconvoluted into 4 peaks, corresponding to Al $2p_{3/2}$, Al $2p_{1/2}$, and a peak due to the formation of a small amount of Al_2O_3.

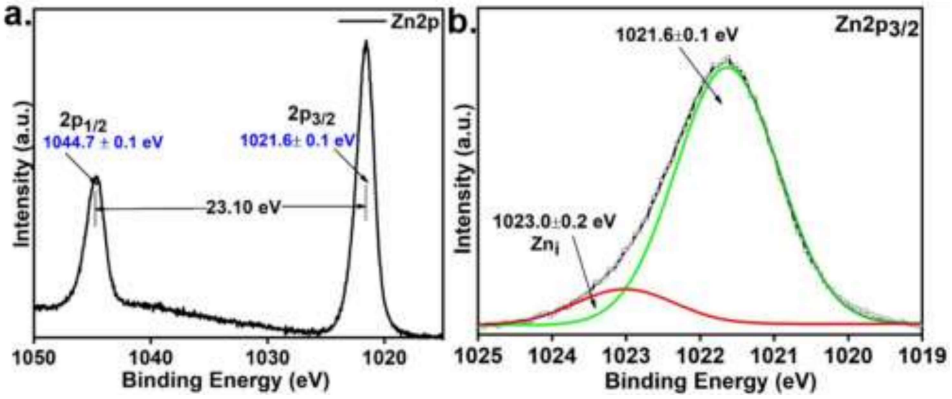

Figure 4.6 Scanned peaks and fitted shoulder peaks on higher binding energy side (a) Zn2p and, (b) Zn $2p_{3/2}$ orbitals

Peaks observed at binding energies of 72.38±0.12 eV and 73.6±0.1 eV were attributed to Al $2p_{3/2}$ and Al $2p_{1/2}$ respectively, arising from the Al at Zn sites [237,238],

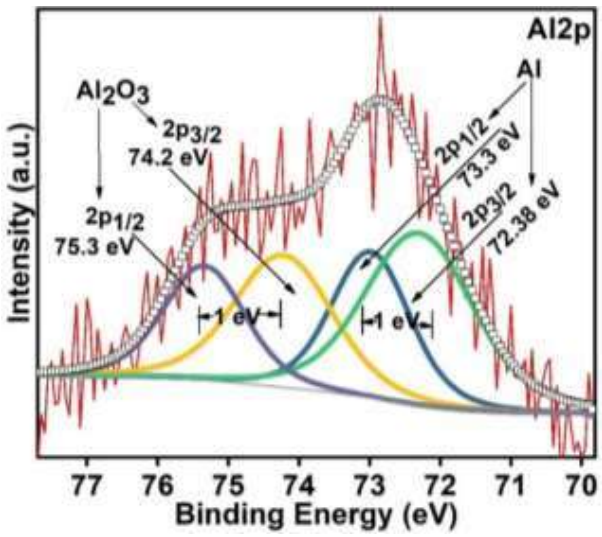

Figure 4.7 Wide scan XPS spectrum of Al 2p core level AZO thin film doped with 1 at% Al

while the pair of peaks at 74.2±0.2 eV and 75.3±0.2 eV attributed to the formation of aluminum oxide[237,239]. This confirmed the presence of a small amount of alumina probably at the grain boundaries, which probably was the main reason for reducing grain (**Figure 4.7**).

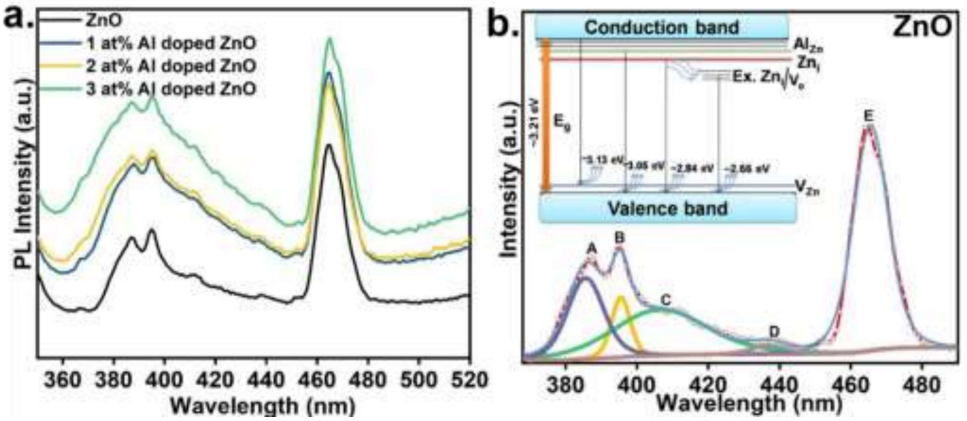

Figure 4.8 Photoluminescence spectra of a) undoped ZnO and 1-3 at% Al-doped zinc oxide b) deconvoluted peaks of zinc oxide thin film (Inset: Energy band diagram based on deconvoluted peaks)

4.2.6 Photoluminescence spectra

To study the doping level and intra-band defect states generated during annealing, defect-related emissions were analyzed. The PL spectra of all the Al-doped ZnO thin film samples could be deconvoluted to several peaks emanating due to the transition between band edges and the defects and dopant levels. The PL spectra obtained from all the films are depicted in **Figure 4.8a**, while **Figure 4.8b** depicts a fitted PL spectrum of a ZnO film. The PL spectra obtained from the deposited films could be de-convoluted with several luminescence peaks of different

wavelengths: a near band edge emission peak at around ~386 nm (Peak A) assigned to the band edge emission, two violet emission peak at slightly different wavelengths ~396 nm (Peak B) and ~406 nm (Peak C) were assigned to zinc vacancies(V_{Zn}) and Al at Zn sites (Al_{Zn}), respectively a relatively weaker violet-blue emission peak at ~435 nm was assigned to be due to Zn interstitial defects (Zn_i), while the blue emission peak at ~465 nm (Peak E) could be assigned to the extended Zn interstitial (Zn_i) states or the presence of oxygen vacancies[240–244]. It should be noted the presence of Zn_i was also confirmed by XPS (**Figure 4.6b**). The deconvoluted luminescence peaks emanating from several intra-band defects are schematically depicted in **Figure 4.8b**. Based on the PL spectra analysis, a band diagram of the AZO was constructed (shown in the inset of **Figure 4.8b**. Relative intensity (normalized against band edge emission) of luminescence peaks changed with Al doping concentration. It is expected that with increased Al-doping, the relative intensity of luminescence peaks associated with Al_{Zn} would increase. At the same time, an increase in Al doping levels decreased the formation energy of zinc vacancy and increased the probability of Al substitution of Zn, and therefore, I_{Zn} (Zn interstitial) sites also increased with Al incorporation in the lattice. The faint emission peak at ~435 nm due to extended states of Zn_i defect did not change much with the dopant concentration. The normalized luminescence intensities emanating from different sites/defect levels as a function of Al doping are depicted in **Figure 4.9**. As expected, the most prominent change due to doping is observed in the luminescence peaks corresponding to the Al_{Zn} and Zn_i sites. The PL intensity corresponding to the Al_{Zn} and Zn_i increased rapidly on increasing Al doping concentration up to 2 at.% while, on further increasing the Al concentration to 3

at.%, the PL intensity reduced for both. The reduction in intensity could be due to Al when added to larger amounts, having a greater tendency for Al_2O_3 formation, as confirmed by XPS. However, it was lower than the detection limit of XRD. The PL intensity emanating from Zn vacancies increased marginally up to 2 at.% Al while increasing substantially on increasing the Al doping to 3 at.% PL peaks emanating from other defects did not change substantially. Since Zn_i sites were greater in numbers and therefore, the intensity of PL emanating from Zn_i was much greater than other PL peaks.

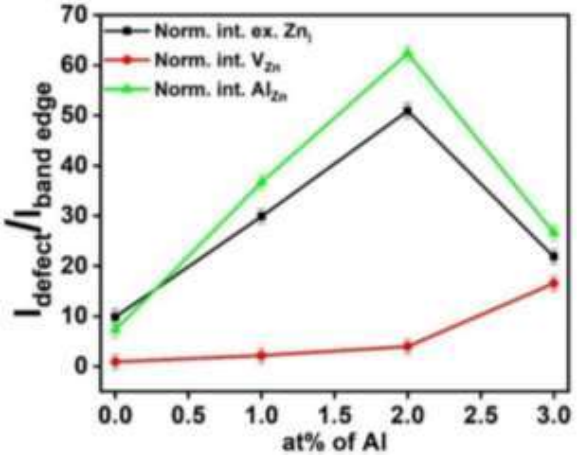

Figure 4.9 PL peak intensity normalized to the band edge PL intensity as a function of Al concentration

4.2.7 Electrical properties of the film

The electrical properties of the films were measured by the Hall-effect measurement system using the Van der Pauw method. The variation in charge concentration, mobility, and resistivity as a function of Al concentration is depicted in **Figure 4.10**. The resistivity decreased, while the bulk carrier concentration increased with

increasing Al concentration up to 2 at.%. On increasing the Al concentration to 3 at.%, the carrier concentration decreased while the resistivity increased drastically. This had a direct correlation with the PL results where the concentration of Al_{Zn} and Zn_i sites increased with Al concentration up to 2 at.% while reduced in increased Al concentration of 3 at.%. The resistivity of films would reduce with increasing charge carrier concentration and mobility. However, it has been established that increasing charge concentration beyond the order of 10^{21} cm^{-3} reduces mobility [245]. In this case, the maximum charge carrier concentration of the order of $10^{19}cm^{-3}$ was obtained for 2 at.% Al doping. Charge carrier mobility decreased progressively on Al doping (from ~32.5 $cm^2V^{-1}s^{-1}$ for pure ZnO to ~9.7 $cm^2V^{-1}s^{-1}$ for 3 at.% Al doping). On doping of Al up to 2 at.%, resistivity decreased to ~$1.2x10^{-2}$ Ω-cm, while on further increasing the dopant concentration to 3 at.%, the resistivity increased to ~$14.89x10^{-2}$ Ω-cm, mainly due to reduced charge carrier concentration. The lowest resistivity of ~$1.2x10^{-2}$ Ω-cm was obtained with 2 at.% Al-doped ZnO. The results obtained compared well with the earlier reported resistivity values for spin-coated films on insulating/transparent substrates having transparency >85%. This is among the best achieved AZO thin film on the amorphous glass substrates. Earlier researchers have obtained lower resistivity values for spin-coated films; however, most of them were achieved either on much thicker films or semiconducting/crystalline substrates. For instance, the least resistivity reported so far using solution-based processing deposited by spin coating is of the order of 10^{-5} Ω-cm. However, that was demonstrated on a micron-thick film having a transparency of less than 50% [246]. Other authors have achieved lower resistivity values in the order of 10^{-3} Ω-cm on semiconducting silicon

substrates or crystalline substrates such as quartz, sapphire, and corning glass, which conduction aid or favors the preferential growth in [002] direction [187,244,247–251]. Vacuum-based deposition techniques such as rf-sputtering [251] and PLD [14] have been demonstrated to deposit high-quality AZO films with resistivities in the order of 10^{-4}-10^{-3} Ω-cm [252]. However, the solution-processed films generally have fewer carriers and lower mobility, thereby, resulting in greater resistivities in the order of 10^{-3}-10^{-2} Ω-cm. The lowest resistivity in the ~10^{-4} Ω-cm reported for solution-deposited AZO films was achieved by Tang and Cameron[218]. However, this was achieved after vacuum annealing, which is known to temporarily create oxygen vacancies.

The absence of preferred orientation in the films deposited on glass substrates using spin coating, coupled with the greater defect concentration and presence of Al_2O_3 in the vicinity of grain boundaries could be the major reason for the lower conductivity values when compared to the films deposited using vacuum-based techniques.

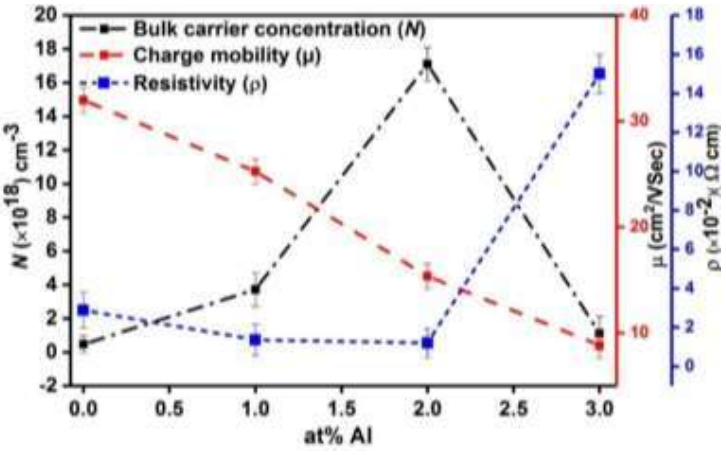

Figure 4.10 Electrical properties of undoped and 1-3 at% Al-doped zinc oxide

The resistivity values in the order of ~10^{-2} Ω-cm with transparency >85% is one of the best results achieved using sol-gel spin coating on a glass substrate. A conductivity value in the order of ~10^{-2} Ω-cm was obtained for the AZO films spin-coated on glass substrates having a thickness of ~150 nm. We have obtained resistivity in the order of ~10^{-2} Ω-cm on a glass substrate with film transparency above ~85%. The effect of different aluminum concentrations (0-3 at.%) was observed, and it was conceived that 2 at% Al was better than other concentrations having a bandgap of 3.18 eV. XRD patterns and SEM images supplemented each other, as the Al concentration increased, the crystallite size and the grain size decreased. With an increase in the Al concentration, the compactness of films also increased, while the roughness decreased. XPS spectrum confirmed the doping of Al in the ZnO lattice. Photoluminescence of Al-doped zinc oxide thin film indicated the presence of Zn interstitials, and it was also shown that an increase in Al concentration leads to an increment in carrier concentration, which is reduced after the addition of more than 2 at.% Al. This was attributed to the formation of greater amounts of Al_2O_3 at the grain boundaries resulting in a reduction in conductivity. Both scanning Kelvin probe microscopy and photoluminescence confirmed the presence of defects and localization at grain boundaries.

4.3 Concluding Remarks

A conductivity value in the order of 10^{-2} Ω-cm was obtained for the AZO films spin-coated on glass substrates having a thickness of ~150 nm. We have obtained resistivity in the order of ~10^{-2} Ω-cm on a glass substrate with film transparency above ~85%. The effect of different aluminum concentrations (0-3 at.%) was

observed, and it was conceived that 2 at% Al was better than other concentrations having a bandgap was 3.18 eV. The XRD patterns and SEM images supplemented each other, as the Al concentration increased, the crystallite size and the grain size decreased. With an increase in the Al concentration, the compactness of films also increased, while the roughness decreased. XPS spectrum confirmed the doping of Al in the ZnO lattice. Photoluminescence of Al-doped zinc oxide thin film indicated the presence of Zn interstitials, and it was also shown that an increase in Al concentration lead to an increase in carrier concentration, which was reduced after the addition of more than 2 at.% Al. This was attributed to the formation of greater amounts of Al_2O_3 at the grain boundaries resulting in a reduction in conductivity. Both scanning Kelvin probe microscopy and photoluminescence confirmed the presence of defects and localization at grain boundaries. Utilizing oxygen-free Al-precursor and annealing in a controlled atmosphere to suppress the formation of Al_2O_3 and reducing the grain boundaries resistance could be the way forward for scale implementation of solution-based processing of TCOs.